Journal of Applied Polymer Science

Design of XNBR Nanocomposites for Underwater Acoustic Sensor Applications: Effect of MWNT on Dynamic Mechanical Properties and Morphology

K. Sasikumar,[1] N. R. Manoj,[1] T. Mukundan,[1] D. Khastgir[2]

[1]Materials Science Division, Naval Physical and Oceanographic Laboratory (DRDO), Thrikkakara, Kochi 682 021 Kerala, India

[2]Rubber Technology Centre, Indian Institute of Technology, Kharagpur 721 302 West Bengal, India

Correspondence to: D. Khastgir (E-mail: khasti@rtc.iitkgp.ernet.in)

ABSTRACT: In this work, application of rubber-MWNT nanocomposite for underwater acoustic sensors is explored. The nanocomposite is developed by incorporating multiwalled carbon nanotubes (MWNT) into carboxylated nitrile rubber by mechanical mixing. The addition of MWNT up to 10 phr is found to result in about 330% increase in tensile strength, 140% increase in modulus, and 160% increase in tear strength. Transmission electron microscopy and scanning electron microscopy analyses indicate uniform dispersion of nanotubes in the rubber matrix. Dynamic mechanical analysis shows that damping at ambient temperature gradually increases with increasing filler content. This is attributed to the augmented frictional energy loss at the interface. The damping peak position shifts upward with increase in MWNT concentration, which may be gainfully used to tune to the operational frequency range of underwater acoustic sensors. Payne effect is observed at higher filler concentration due to the breakage of aggregates formed by filler–filler interaction. The nanocomposite may find application for damping structural vibrations and thus to improve the performance of underwater acoustic sensors. © 2014 Wiley Periodicals, Inc. J. Appl. Polym. Sci. **2014**, *131*, 40752.

KEYWORDS: composites; graphene and fullerenes; mechanical properties; microscopy; nanotubes; rubber

Received 20 January 2014; accepted 22 March 2014

DOI: 10.1002/app.40752

INTRODUCTION

Underwater acoustic sensors are used in civilian and military applications for detecting and locating the presence of submerged objects as well as finding/harvesting fish groups, by emitting and receiving acoustic energy.[1] The frequency range may vary from 20 Hz to 1 MHz depending on the application. Piezoelectric materials are widely used in these acoustic sensors for reception of sound waves and to convert it to electrical signals. Whenever such sensors are fitted on a platform, they are prone to vibrations of the platform and unwanted noise, which in effect reduces the efficiency of sensing and thus would necessitate complex signal processing. Various types of isolators and damping treatments are widely used to improve the signal-to-noise ratio of underwater sensors by isolating or decoupling structure-borne noise emanating from a ship's hull, and by providing a proper impedance backing for one or more sensors.[2,3] Polymer composites having good damping characteristics are often used for the development of this type of vibration isolators. The standard methodology is by the introduction of damping as it reduces structural vibrations and consequent noise levels, while improving structural integrity and longevity. Elastomeric polymers, due to their inherent viscoelastic nature, undergo segmental motion and dissipate incoming vibration energy in the form of low magnitude heat. Many attempts are made to tune the damping nature and strength. Two widely used methods are the modification of polymer matrix and addition of high damping fillers.[4,5]

Conventionally, reinforcing fillers such as carbon black and silica are used to improve the mechanical strength of rubber compounds. However, these fillers need to be added in quite large quantity, which adds a weight penalty, and in some cases affects the inherent polymer properties. In recent years, nanomaterials have become the preferred choice of polymer scientists to design lightweight composites,[6,7] which are known as polymer nanocomposites. Due to the high surface area of nanomaterials, one can achieve enhanced filler–matrix interaction at a significantly lower level of filler loading, compared to the conventional fillers. The incorporation of nano-fillers is also found

This article was published online on 09 April 2014. An error was subsequently identified. This notice is included in the online and print versions to indicate that both have been corrected 17 April 2014.

to increase the thermal stability significantly.[8] Nanoclay has been widely used in many polymer materials to improve various properties.[9] Addition of nanoclay into nitrile rubber is found to increase the tensile strength significantly due to the reinforcing action.[10] Carbon nanotubes (CNT), due to very high mechanical properties and other exotic functional properties, have become prime candidates for many novel applications.[11–13] Particularly multi-walled carbon nanotubes (MWNT) have attracted the researchers more due to the low production cost and high performance. Addition of MWNT is found to induce electrical conductivity in styrene–butadiene–styrene (SBS) block copolymer, due to the hopping of charges between adjacent nanotubes.[14] The DC and AC electrical resistivity of polyethylene is found to decrease with the increase of CNT loading.[15] MWNT also improves the rheological properties in polystyrene nanocomposites due to better interaction with the matrix.[16] Interestingly, CNT nanocomposites are found to have better vibration damping capability also.[17] Numerical simulations showed that damping ratio can be boosted by adding a small amount of CNT into polymer matrix.[18,19] The energy absorption in nanocomposites of MWNT is explained by considering the interfacial stick-slip motion between the matrix and nanotubes.[20,21]

In the present work, the development of MWNT-based rubber nanocomposites is detailed, aimed particularly for damping low frequency structural vibrations of the order of 100–1000 Hz. Carboxylated nitrile rubber (XNBR) is chosen as the matrix considering its unique possession of a combination of high mechanical and abrasion properties along with high damping properties.[22] It is a high performance specialty rubber having pendant carboxyl groups at random along the macromolecular chain. Though XNBR can be crosslinked either covalently or ionically, covalent crosslinking method has been chosen here to get better compression set.[23] The nanocomposites are characterized in detail for mechanical and dynamic mechanical properties. The morphology is studied by scanning electron microscopy (SEM) and transmission electron microscopy (TEM). The strain dependent properties and damping capabilities are analyzed by dynamic mechanical analysis (DMA).

EXPERIMENTAL

Materials and Methods

Sample Preparation. Nanocomposites were prepared using XNBR (Chemigum NX-146, ML 1+4[100°C]: 45 ± 5, acrylonitrile content: 33%, carboxylic acid content: 1.0%, Eliochem, India) as matrix and MWNT (supplied by M/s Chemapol, Mumbai; purity: 95%; average diameter: 10–20 nm; length: 5–10 microns). Two methods are commonly adopted to incorporate nanotubes into rubber matrix, namely solution mixing and dry mixing in a two-roll mill. Initially, solution mixing method was attempted to prepare nanocomposites. However, in this method quantity of solvent required to dissolve the rubber was large, (about 2000 mL for 100 g of rubber) and complete removal of solvent posed a challenging task. The presence of even traces of solvent was found to decrease the mechanical properties significantly. Hence the alternative method of dry mixing in two-roll mill was adopted. MWNT was incorporated immediately after mastication of rubber, followed by the other compounding ingredients to ensure better dispersion of nanotubes. This method is found to improve the mechanical properties substantially.

The compound recipe included 5 phr (parts per hundred rubber) zinc oxide, 2 phr stearic acid, 1.5 phr *n*-cyclohexyl-2-benzothiazole-sulfenamide (CBS), and 3 phr sulfur along with different loading levels (0, 1, 3, 5, 7, 10 phr) of MWNTs. Incorporation of MWNT beyond 10 phr by mill mixing became a difficult task and hence the loading level was limited upto 10 phr. Compounding was done in a laboratory size two-roll mixing mill having a friction ratio of 1 : 1.2. The stocks were cured under pressure at 150°C to 2 mm thick sheets.

Characterization. ***Morphology.*** TEM (JEOL 3010) and SEM (FEI Quanta FEG 200—High Resolution) were used to characterize the morphology.

Mechanical properties. Tensile properties were evaluated according to ASTM standard D 412-98 using dumbbell-shaped specimens in a universal testing machine (UTM) model ZWICK 1476, Germany at a constant crosshead speed of 500 mm/min at room temperature. *E*-Modulus was determined in the low strain region of 0.25%–2%. Tear strength was evaluated according to ASTM standard D 624-00 on Type C test specimens in UTM.

Dynamic mechanical properties. DMA was carried out on DMA Q 800 (TA instruments, USA) in tensile mode using test specimens of dimension 20 mm × 4 mm × 2 mm. Three types of experiments, viz. temperature ramp at constant frequency, frequency sweep at various temperatures, and isothermal strain amplitude sweep experiments were conducted.

In temperature ramp experiment, the test specimen was subjected to a sinusoidal oscillation at a constant frequency of 1 Hz at a heating rate of 3°C/min from −50 to +50°C. The storage modulus (E') and loss factor (tan δ) were measured as a function of temperature for all of the samples under identical conditions. The glass transition temperature (T_g) of the samples was calculated from the respective tan δ peak positions. In frequency sweep experiment, the test specimen was subjected to a series of sinusoidal oscillations at discrete frequencies (0.5, 1, 2, 5, 10, 20, and 50 Hz) at various temperature steps in the range −50°C to +50°C. In isothermal strain amplitude sweep experiment, sample specimens were subjected to a sinusoidal vibration having frequency of 1 Hz and strain amplitude was varied from 0 to 1000 μm at a constant temperature of 25°C and the change in storage modulus was measured to study Payne effect.

In all these experiments, a minimum of three test specimens were tested and the average was taken. The percentage error is less than 2% in all cases except for elongation at break (EB), where it is about 5%.

RESULTS AND DISCUSSION

Mechanical Properties

The tensile stress–strain plots of neat XNBR and nanocomposites are shown in Figure 1. The increase in the slope of stress–strain curves with increase in filler loading indicates steady

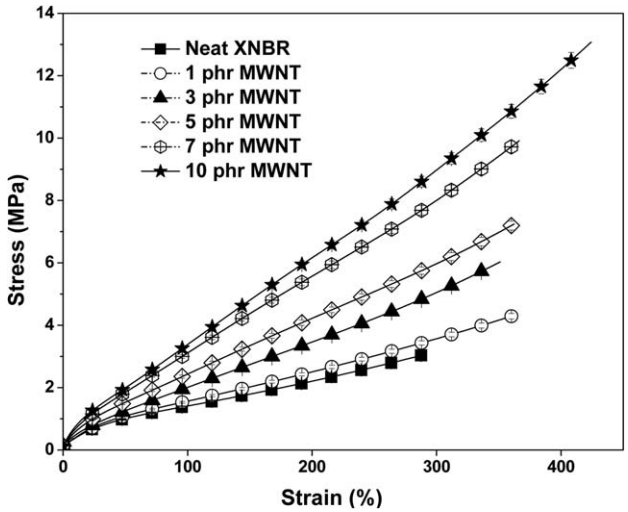

Figure 1. Stress–strain plots of neat XNBR and nanocomposites.

improvement of reinforcement. However, the maximum concentration of filler is kept at 10 phr, due to the difficulty in the incorporation of MWNT in XNBR matrix by mill mixing, beyond 10 phr. The mechanical properties namely, tensile strength, *E*-modulus, modulus at 100% elongation, EB, and tear strength are presented in Table I. It can be observed that as the CNT content in composites increases, modulus and tensile strength increase gradually indicating better polymer–filler interaction. At 3 phr level, the tensile strength doubles and at 10 phr it becomes three times that of neat XNBR. Overall, there is about 330% increase in tensile strength, 140% increase in *E*-modulus, and 160 % increase in tear strength due to the addition of upto 10 phr MWNT.

This kind of significant increase in the tensile properties cannot be observed at low loading levels of conventional fillers like carbon black, where the standard loading range varies from 30 to 70 phr.[24] Exceptional reinforcement at a low loading of CNT is attributed to the high aspect ratio (*L*/*D*) of CNT, which leads to trapped entanglements of the polymer chains around the nanotubes forming physical crosslinks.[25] Further, affinity between nanotubes and polar groups present in XNBR namely nitrile (—CN) and carboxylic (—COOH) groups also brings in improved polymer–filler interaction.[26] Another interesting observation is the increasing trend of EB along with tensile strength as the filler loading increases. This behavior is typical of nanocomposites, as opposed to common composites with fillers in the micrometer range.[27] Micron sized fillers usually increase the strength at the cost of ductility as they act as stress concentrators. Nano-sized fillers, if well dispersed, on the other hand, provide simultaneous strengthening and toughening.[28] Tear strength also increases with increase in filler loading.

The key advantage of these composites is in the enhancement in mechanical properties without much increase in density. The increase in density will lead to higher acoustic impedance which is undesirable for efficient transfer of acoustic energy from the sensor to the medium or vice versa.

Morphology Study by SEM

The tensile fractured surfaces of neat XNBR and nanocomposites were viewed using SEM at low magnification (×60) and high magnification (×15,000), as shown in Figures 2 and 3. The low magnification permits a clear overview of the samples for easy comparison. At low magnification, the tensile fractured sample of neat XNBR matrix [Figure 2(a)] shows a plain surface whereas the nanocomposites show layered fracture surfaces with an array of parabolic markings [Figure 2(b–d)]. The increased interaction between matrix and MWNT is evident from the increased number of markings at higher filler loading.

At higher magnification also neat XNBR matrix [Figure 3(a)] shows relatively plain surface, whereas the nanocomposites [Figure 3(b–d)] show glowing worm-like structures of MWNT dispersed evenly throughout the matrix. The image [Figure 3(d)] corresponding to the composite with 10 phr MWNT shows more undulated and rippled surface indicating good interaction between the matrix and MWNT. A few outcrops of the CNT are also observable on the fractured surfaces indicating the existence of strong interaction between nanotubes and XNBR.

Morphology Study by TEM

TEM images of ultramicrotomed samples of nanocomposites are shown in Figure 4(a–d). These images indicate uniform dispersion of MWNT in the rubber matrix. Moreover, cluster formation and entanglement of nanotubes are also observed at higher filler loadings. Nanocomposite with 1 phr MWNT loading shows uniformly long CNTs whereas others show significantly shorter nanotubes. The breakage of the nanotubes at higher filler loading levels is expected due to the increased shearing force experienced during mill mixing.[28] In fact, this

Table I. Mechanical Properties of Neat XNBR and Nanocomposites

MWNT loading (phr)	Density (g/cm^3)	Tensile strength (MPa)	*E*-modulus (MPa)	Modulus at 100% (MPa)	Elongation at break (%)	Tear strength (N/mm)
0	1.03	2.9	3.6	1.4	300	8.6
1	1.03	4.2	4.0	1.6	330	14.2
3	1.04	6.0	4.7	2.1	345	19.5
5	1.05	7.1	5.9	2.4	359	21.0
7	1.06	9.8	7.4	3.0	370	21.6
10	1.07	12.6	8.5	3.4	420	22.5

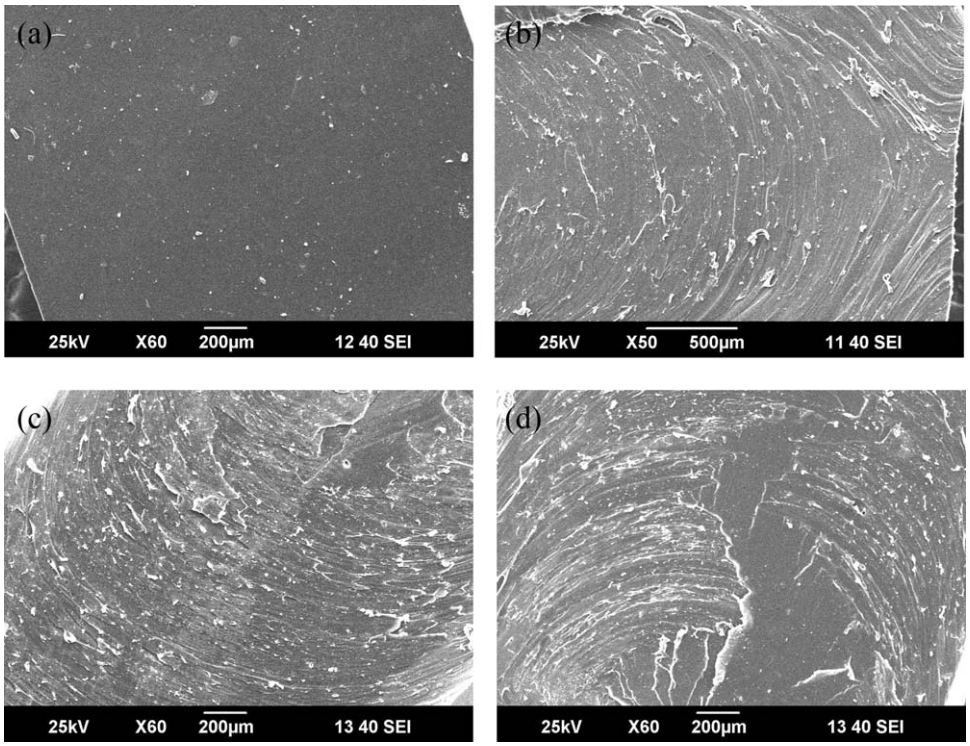

Figure 2. SEM images of tensile fractured surfaces at low magnification: (a) Neat XNBR; (b) XNBR + 3 phr MWNT; (c) XNBR + 5 phr MWNT; (d) XNBR + 10 phr MWNT.

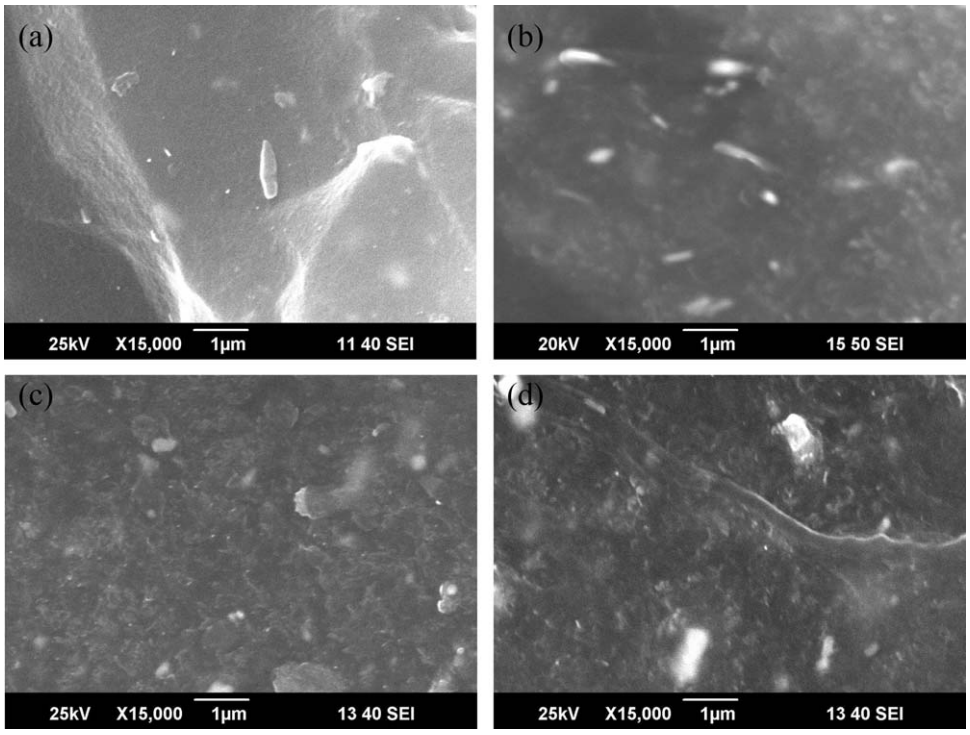

Figure 3. SEM images of tensile fractured surfaces at high magnification: (a) Neat XNBR; (b) XNBR + 3 phr MWNT; (c) XNBR + 5 phr MWNT; (d) XNBR + 10 phr MWNT.

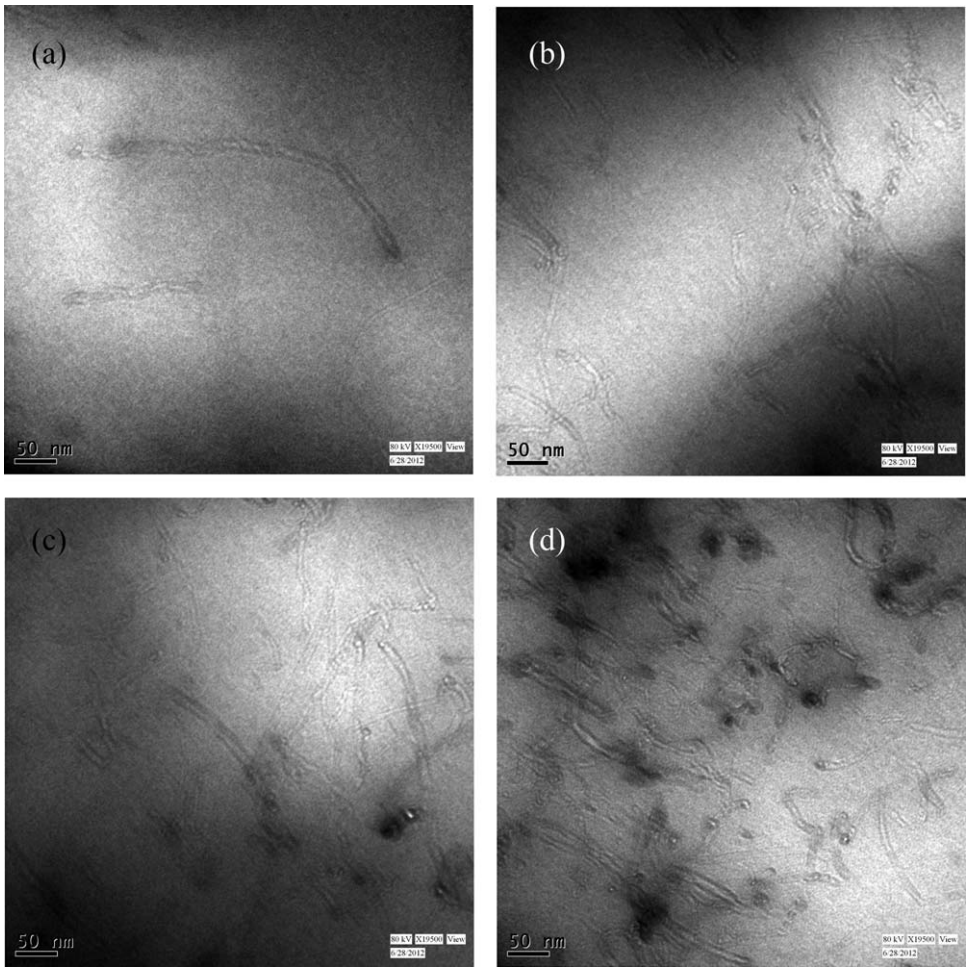

Figure 4. TEM images of nanocomposites: (a) XNBR + 1 phr MWNT; (b) XNBR + 3 phr MWNT; (c) XNBR + 5 phr MWNT; (d) XNBR + 10 phr MWNT.

corroborates the prediction of low effective aspect ratio by Guth–Smallwood equation and the occurrence of Payne effect at higher filler loadings, as explained further.

Dynamic Mechanical Analysis

Temperature Ramp Experiment. The storage modulus (E'), loss modulus (E''), and tan δ as a function of temperature in the range −50 to +50° C are evaluated by temperature ramp

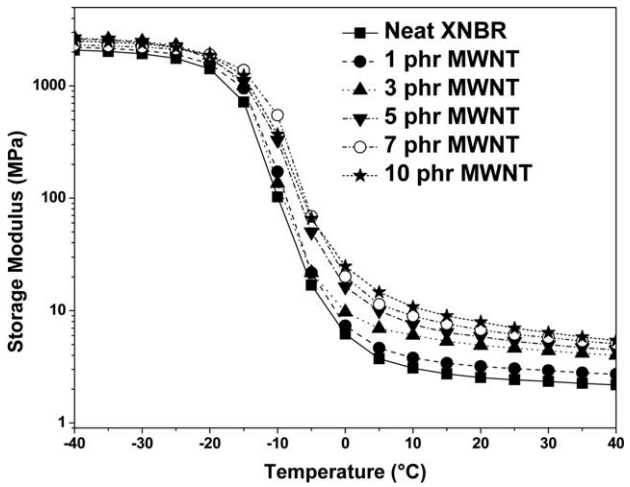

Figure 5. Dynamic storage modulus vs. temperature plot of neat XNBR and nanocomposites.

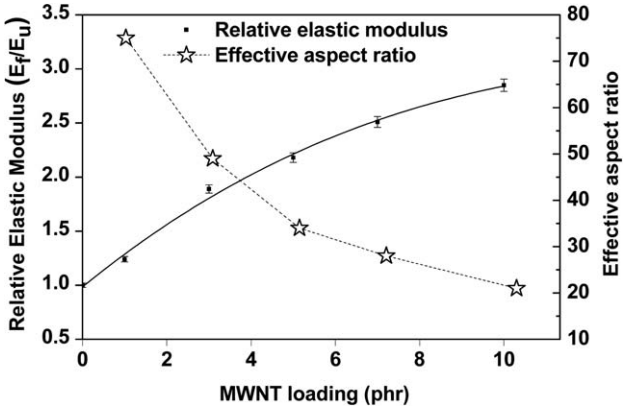

Figure 6. Relative elastic modulus and effective aspect ratio vs MWNT loading plot of neat XNBR and nanocomposites.

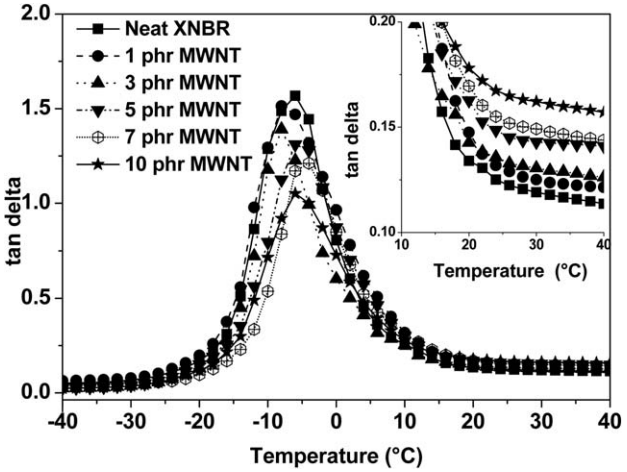

Figure 7. Tan δ vs. temperature plot of neat XNBR and nanocomposites.

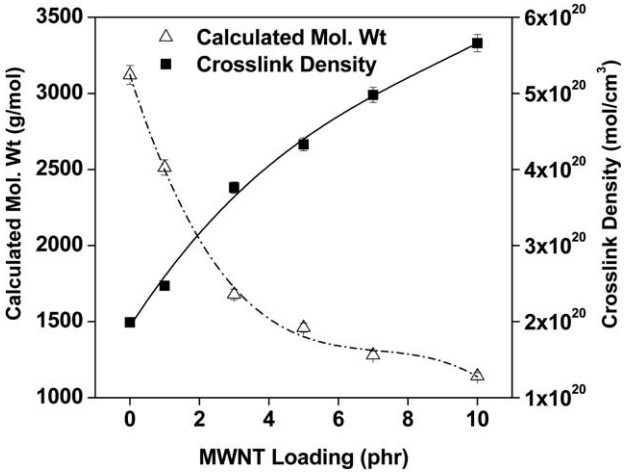

Figure 8. Molecular weight and crosslink density vs. MWNT concentration plot of neat XNBR and nanocomposites.

experiment. The E' (Figure 5) is found to increase with the increase in MWNT loading, throughout the temperature range, due to the hydrodynamic reinforcement effect of the high modulus filler.[29] The values of E' at 25°C are further investigated using Guth–Smallwood[30,31] equation [eq. (1)]

$$E_f/E_u = 1 + 0.67fv_f + 1.62f^2v_f^2 \quad (1)$$

where E_f is elastic modulus of the filled rubber, E_u is elastic modulus for unfilled rubber, f is the aspect ratio, and v_f is the volume fraction of the filler. The ratio of E_f/E_u (relative elastic modulus) is found to increase with increase in MWNT loading (Figure 6). The effective aspect ratios of the nanotubes in the composites were calculated from the relative elastic modulus using eq. (1). It varies from 75 for nanocomposite with 1 phr MWNT to 20 for composite with 10 phr MWNT (Figure 6). The calculated aspect ratio is much lower than the actual aspect ratio of pristine MWNT (~500–1000). The huge difference is attributed to the agglomerate formation as well as the breakage of MWNTs during mill mixing. The breakage of nanotubes is prominent in the case of nanocomposites having higher loading of CNT (5 phr and above), as observed in TEM analysis [Figure 4 (c,d)].

Tan δ, the ratio of E'' to E', shows a decreasing trend with increasing filler content at low temperatures upto T_g (Figure 7). Interestingly, above T_g, tan δ increases with increase in MWNT concentration (Figure 7 insert). This opposing trend of tan δ at low and high temperatures can be explained by considering the immobilization of the macromolecules by the nanotubes. The enhanced polymer–filler interaction reduces the segmental mobility of polymer chains in the nanocomposites. Immobilization results in higher hysteresis (higher tan δ) at higher temperatures and lower hysteresis (lower tan δ) at lower temperatures.[32]

To confirm the formation of physical crosslinks and improved polymer–filler interaction, the crosslink density of the composites was determined from dynamic modulus at room temperature and density, using eq. (2).

$$E = \frac{3\rho RT}{M_c} \quad (2)$$

where E is dynamic modulus at 298 K, ρ is density, R is universal gas constant, T is temperature (298 K), and M_c is molecular mass between crosslinks. The crosslink density (V_c) is calculated from eq. (3).

$$V_c = \frac{\rho N}{M_c} \quad (3)$$

where N is Avogadro's number.

The results are shown in Figure 8. It is seen that with increase in filler loading, the effective molecular weight decreases whereas the crosslink density increases, both in the order of 3rd order polynomial. Even though the quantity of vulcanization agents used is same in all the cases, the trapped entanglements of polymer chains around nanotubes act as physical crosslinks resulting in higher crosslink density and thereby higher modulus and hysteresis.

Frequency Sweep Experiment and Time Temperature Superposition. Due to the wide operational frequency band (10 Hz to 10 MHz) of underwater acoustic sensors, it is essential to characterize the frequency dependent damping characteristics over a wide frequency range. There is no direct experimental method to evaluate dynamic viscoelastic properties in this wide range of frequency spectrum. Hence the principle of time–temperature superposition is applied using William–Landel–Ferry (WLF) equation[33]:

$$\log a_T = \frac{C_1(T - T_r)}{C_2 + (T - T_r)} \quad (4)$$

where a_T is the shift factor, T_r is the reference temperature, C_1 and C_2 are constants and their general values at T_g are 17.4 and 51.6, respectively. The values calculated from the best fit correlation vary from 9.87 to 20.47 for C_1 and from 81.07 to 112.7 for C_2 in respect of composites containing MWNT content in the range 0–10 phr. Figure 9 shows the master curve generated by

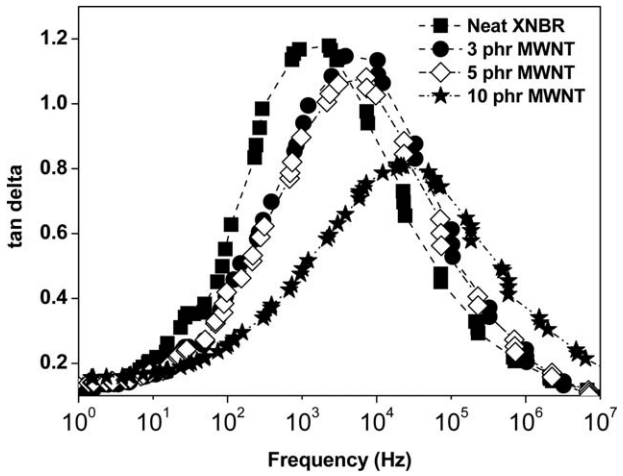

Figure 9. Tan δ vs. frequency plot of neat XNBR and nanocomposites.

time–temperature superposition. The low frequency structural vibrations (below 50 Hz) predominately affect the performance of underwater acoustic sensors due to high amplitudes. Hence, in order to improve the performance of an underwater acoustic sensor, the sensor should be isolated from these low frequency vibrations. From Figure 9, it can be observed that nanocomposites have higher tan δ at low frequencies and hence will be able to damp low frequency vibrations more effectively than the neat XNBR. At the same time, nanocomposites have tan δ lower than the neat XNBR in the frequency range of 100 Hz to 10 kHz. This is an added advantage, because the nanocomposites will be acoustically transparent, resulting in minimum transmission loss in this frequency range. Further, the tan δ peak position is seen to shift upward on the frequency scale with increase in the MWNT concentration, which can be used to judiciously tune the operational frequency range by merely changing the composition. Considering the overall improvement in damping in selective frequency ranges, various types of mounts and decouplers can be made with these nanocomposites to suit the underwater sensor applications.

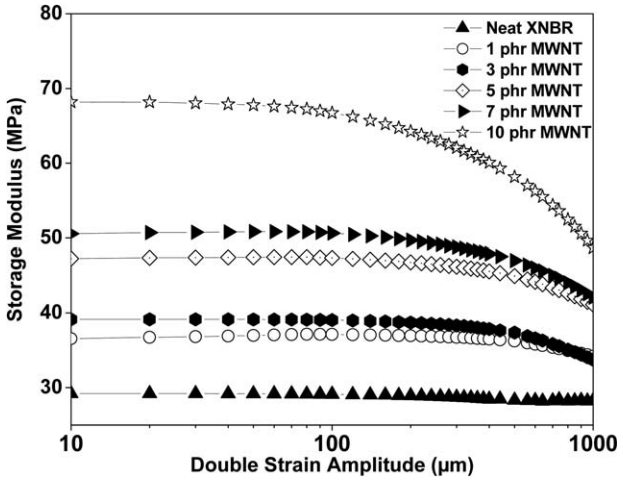

Figure 10. Storage modulus vs. double strain amplitude plot of neat XNBR and nanocomposites.

Amplitude Sweep Experiment. The Payne effect is a special characteristic of filled rubber, where the increase in strain amplitudes leads to decrease in storage modulus. It is attributed to the breakage and reformation of weak physical bonds between the filler aggregates.[34] The existence of Payne effect in the nanocomposites is assessed by determining the E' as a function of double strain amplitude (Figure 10). In the case of neat XNBR and nanocomposites up to 3 phr loading, E' does not decrease significantly with increase in the strain amplitude. As the filler loading increases, the low strain E' is considerably higher than that of neat matrix and it decreases with increase in the strain amplitude indicating breakage of filler agglomerates formed. This is prominent in the case of 10 phr loading. The agglomeration can be seen in the TEM images also [Figure 4(c,d)]. However, the overall modulus of highly loaded composite is still higher than the neat matrix due to the combined effect of polymer–polymer entanglements, elastically effective filler–polymer couplings, and the hydrodynamic effect.

CONCLUSIONS

In this work, a polymer nanocomposite is developed by incorporating MWNT into XNBR by mechanical mixing, especially for damping applications. The nanocomposites show about 330% increase in tensile strength, 140% increase in *E*-modulus, and 160% increase in tear strength due to the addition of up to 10 phr MWNT. Electron micrographs indicate uniform distribution of nanotubes in the composites. Damping, as studied by dynamic mechanical analysis, gradually increases with increasing MWNT content due to the increasing frictional energy loss at the interface. In the frequency domain, damping peak position shifts upward with increase in MWNT concentration, which is advantageous and helpful to tune the operational frequency range of underwater acoustic sensors. At very high concentration, aspect ratio of nanotube is found to decrease due to breakage of nanotubes, as studied by Guth–Smallwood model also. Payne effect is observed at higher filler concentration due to the breakage of aggregates formed by filler–filler interaction. The combination of good tensile properties along with excellent damping over a wide range of frequencies make the nanocomposites suitable for vibration damping applications in general and for underwater acoustic sensors in particular.

ACKNOWLEDGMENTS

The authors wish to thank Director, Naval Physical and Oceanographic Laboratory for providing necessary support to carry out this work and granting permission to publish this work in this journal. The authors also thank Director, Indian Institute of Technology, Kharagpur for providing TEM & SEM facilities.

REFERENCES

1. Urick, R. J. Principles of Underwater Sound, 3rd ed.; Peninsula Publishing: Los Altos, 1983.
2. Capps, R. N.; Thompson, C. M. Handbook of Sonar Transducer Passive Materials; National Research Laboratory: Washington DC, **1981**.

3. Boroditsky, L. In Proceedings of EuroNoise, 6th European Conference on Noise Control, Tampere, Finland, **2006**.
4. Liu, Q. X.; Ding, X. B.; Zhang, H. P.; Yan, X. *J. Appl. Polym. Sci.* **2009**, *114*, 2655.
5. Ibarra, L.; Rodríguez, A.; Mora, I. *Eur. Polym. J.* **2007**, *43*, 753.
6. Perez, L. D.; Giraldo, L. F.; Brostow, W.; Lopez, B. *E-Polymers* **2007**, *29*, 1.
7. Zhou, X. W.; Zhu, Y. F.; Liang, J. *Mater. Res. Bull.* **2007**, *42*, 456.
8. Choudhury, A.; Bhowmick, A. K.; Ong, C.; Soddemann, M. *J. Nanosci. Nanotechnol.* **2010**, *10*, 5056.
9. Chan, M.-L.; Lau, K.-T.; Wong, T.-T.; Ho, M.-P.; Hui, D. *J. Compos. B* **2011**, *42*, 1708.
10. Soares, B. G.; Oliveira, M. d.; Zaioncz, S. *Polímeros* **2010**, *20*, 371.
11. Meyyappan, M. Carbon Nanotube: Science and Applications; CRC Press: Florida, **2005**.
12. Iijima, S. *Nature* **1991**, *354*, 56.
13. Das, N. C.; Maiti, S. *J. Mater. Sci.* **2008**, *43*, 1920.
14. Sencadas, V.; Simoes, R.; Viana, J. C.; Lanceros-Méndez, S. *J. Mater. Sci.* **2013**, *48*, 1172.
15. Rahaman, M.; Thomas, S. P.; Hussein, I. A.; De, S. K. *Polym. Compos.* **2013**, *34*, 494.
16. Zhang, K.; Lim, J. Y.; Choi, H. J.; Lee, J. H.; Choi, W. J. *J. Mater. Sci.* **2013**, *48*, 3088.
17. Suhr, J.; Koratkar, N.; Keblinski, P.; Ajayan, P. M. *Nat. Mater.* **2005**, *4*, 134.
18. Sun, L.; Gibson, R. F.; Gordaninejad, F.; Suhr, J. *Compos. Sci. Technol.* **2009**, *69*, 2392.
19. Zhou, X.; Shin, E.; Wang, K. W.; Bakis, C. E. *Compos. Sci. Technol.* **2004**, *64*, 2425.
20. Koratkar, N.; Wei, B.; Ajayan, P. M. *Adv. Mater.* **2002**, *14*, 997.
21. Kireitseu, M.; Hui, D.; Tomlinson, G. *Compos. Part B* **2008**, *39*, 128.
22. Bandyopadhyay, S.; De, P. P.; Tripathy, D. K.; De, S. K. *Polymer* **1996**, *37*, 353.
23. Ibarra, L. *J. Appl. Polym. Sci.* **1999**, *73*, 927.
24. Cadambi, R. M.; Ghassemieh, E. *J. Appl. Polym. Sci.* **2012**, *124*, 4993.
25. Basuli, U.; Chaki, T. K.; Chattopadhyay, S.; Sabharwal, S. *Polym. Compos.* **2010**, *31*, 1168.
26. Vaisman, L.; Wachtel, E.; Wagner, H. D.; Marom, G. *Polymer*, **2007**, *48*, 6843.
27. Ajayan, P. M.; Schadler, L. S.; Braun, P. V. Nanocomposite Science and Technology; Wiley-VCH GmbH & Co.: Weinheim, **2003**.
28. Thomas, S. P.; Thomas, S.; Marykutty, C. V.; Mathew, E. J. *J. Polym.* **2013**, 2013, *10*.
29. Vu, Y. T.; Mark, J. E.; Pham, L. H.; Engelhardt, M. *J. Appl. Polym. Sci.* **2001**, *82*, 1391.
30. Guth, E.; Gold, O. *Phys. Rev.* **1938**, *53*, 322.
31. Smallwood, H. M. *J. Appl. Phys.* **1944**, *15*, 758.
32. Lopez Manchado, M. A.; Biagiotti, J.; Valentini, L.; Kenny, J. M. *J. Appl. Polym. Sci.* **2004**, *92*, 3394.
33. Williams, M. L.; Landel, R. F.; Ferry, J. D. *J. Am. Chem. Soc.* **1955**, *77*, 3701.
34. Luo, W.; Hua, X.; Wang, C.; Li, Q. *Int. J. Mech. Sci.* **2010**, *52*, 168.